# Testing Rockwall Closure Effects on the Strength Development of Cemented Paste Backfill

Hongbin Liu[1] and Mamadou Fall[1]

[1]Department of Civil Engineering, University of Ottawa, Ottawa, ON, Canada, hliu254@uottawa.ca, mfall@uottawa.ca

## Abstract

The increasing depth of underground mines, driven by the scarcity of surface ore deposits, has led to higher horizontal ground stresses and subsequent rockwall closure, impacting underground mining operations. Cemented paste backfill (CPB) is commonly used to support excavations, but its response to multiaxial stress conditions in deep mines remains poorly understood. This research addresses this knowledge gap by introducing a new multiaxial compressive stress (MCS) curing and monitoring apparatus for CPB capable of simulating rockwall closure-induced stresses encountered in underground mines. The developed apparatus applies two horizontal stresses ($\sigma_{H1}$ and $\sigma_{H2}$) resulting from rockwall closure and a vertical stress ($\sigma_V$) to CPB samples during curing. Validation tests confirm its efficacy and reliability to replicate rockwall closure conditions. Employing this apparatus, the study investigates how rockwall closure impact strength development of the studied CPBs.

Experimental results indicate that time-dependent multiaxial compressive stresses, including vertical stress from self-weight and rockwall closure-induced horizontal stresses, can significantly enhance the early-age unconfined compressive strength (UCS) of CPB. Specifically, the UCS improvement at curing ages of 1, 3, and 7 days amounts to 29, 58, and 37%, respectively, compared to control samples without multiaxial loadings. This strength enhancement is attributed to the densification of the CPB's pore structure and the acceleration of cement hydration. It is crucial to note that rapidly increasing rockwall closure-induced horizontal stresses at later curing ages have notable contribution to further densification of CPB. Moreover, the study identifies that the horizontal and vertical deformations within CPB are significantly influenced by stress evolution in each axial direction. These findings provide valuable insights into the curing behavior of CPB under rockwall closure-induced stresses, facilitating an improved understanding of CPB performance in deep mining applications. This knowledge is crucial for optimizing backfilling practices, enhancing underground mine safety, and ultimately increasing mining efficiency in deeper ore deposits.

Key words: tailings, deep mines, multiaxial stress curing apparatus, horizontal ground stress, unconfined compressive strength

## Introduction

The increasing depth of underground mining driven by the depletion of shallow ore deposits has ushered in a new set of challenges, including heightened ground stresses and increased temperatures. In response, the CPB technique has emerged as a promising solution for supporting underground mine stopes. Traditionally, CPB design relies on uniaxial compressive strength (UCS) testing under conventional laboratory conditions. However, this approach falls short of capturing the effect of complex *in situ* curing conditions encountered in actual mine settings on the UCS of the CPB.

In recent decades, researchers have developed innovative laboratory apparatus to bridge this gap, simulating *in situ* conditions more closely (Belem et al., 2002, Benzaazoua et al., 2006, Fall and Ghirian 2014, Ghirian and Fall 2016, Cui and Fall 2016, Chen et al., 2021). These apparatuses have proven valuable in understanding the impact of different curing conditions, involving thermal, hydraulic, mechanical, and chemical (THMC) factors, on the curing behaviour of CPB. These devices are constrained to applying one-dimensional stress, with a maximum vertical stress limit of 1000 kPa on the CPB. Thus, a significant knowledge gap still remains, particularly concerning the influence of multiaxial stress curing condition in underground deep mine, where exist the horizontal ground stresses due to

rockwall closures and higher *in situ* vertical stress induced from a greater height of the stope and/or the upper layer of rock, on CPB strength and its stability. In practice underground mining scenarios, stope heights can reach up to 200 m (Masniyom 2009, Grabinsky et al., 2022), leading to significantly higher backfill self-weight pressures that reach ~ 4 MPa or even higher.

Besides the effect of vertical stress, rockwall closures pose an important challenge in underground mines, particularly at considerable depths (Figure 1). Rockwall closure, characterized by the horizontal movement of rock towards the opening face due to horizontal ground stress, results in the convergence of stope walls after excavation. This lateral movement exerts pressure on the backfill, potentially causing crushing and extensional fracturing near the backfill surface. A noteworthy example is the Lucky Friday Mine, extending 2300 m below the surface, where meticulous measurements using specialized closure meters reveal stope closures > 50 cm and horizontal backfill stresses reaching up to 5.5 MPa (Seymour et al., 2016, 2017, 2019, Raffaldi et al., 2019). As mining operations extend deeper, rockwall closures worsen. Hartebeestfontein Mine, > 3000 m deep, experienced closures at 6 mm/day for 37 days (Malan and Basson 1998), with an average maximum horizontal stress of 9.0 MPa (Arnold 1993). Despite the urgency, no prior research has explored how time-dependent rockwall closures impact CPB curing behavior and key design properties (eg, strength, deformation, self-desiccation). The research gap is mainly caused by a lack of suitable experimental equipment to mimic time-dependent MCS curing environments in deep mines.

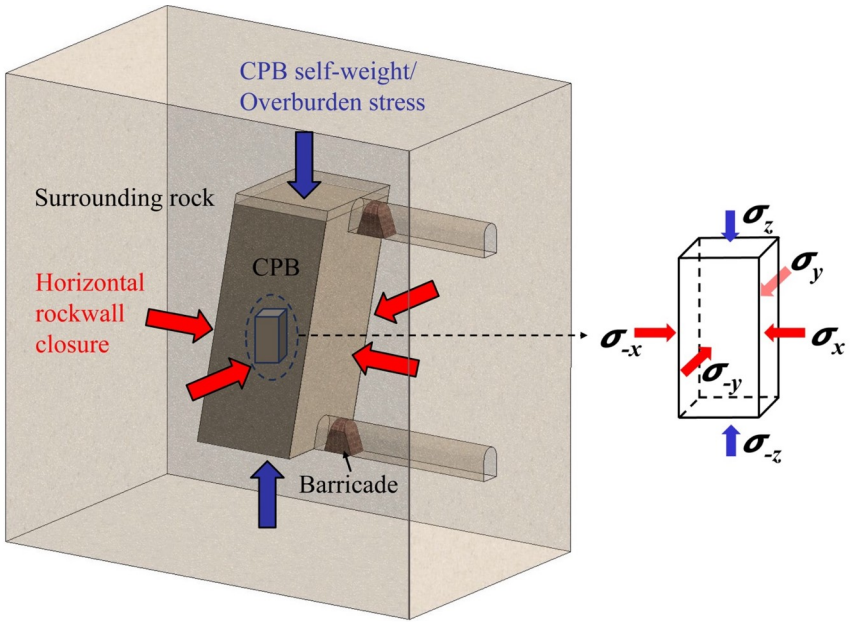


Figure 1. Schematic diagram of the interaction between CPB and surrounding rock.

This paper addresses this gap by introducing a new laboratory apparatus capable of simulating MCS conditions, including rockwall closure-induced horizontal stresses and vertical self-weight or overburden stresses. As well, it investigates the effect of MCS curing conditions on CPB strength development. Unlike existing devices, this apparatus allows for time-dependent multiaxial compressive loading and the monitoring of key engineering properties of CPB during the curing process in deep mine conditions, including multiaxial deformation and self-desiccation. In addition, this study determines critical properties of CPB at specific curing times, such as strength and physical characteristics, under the time-dependent multiaxial compressive loading. This research endeavors to shed light on the intricate impact of MCS conditions in deep mines, and on the curing behavior of the CPB while offering insights crucial for optimizing CPB performance and enhancing safety and efficiency in underground mining applications.

**Apparatus Structure and Key Features**

The apparatus for curing and monitoring CPB under MCS loadings plays a crucial role as a versatile tool for simulating MCS curing conditions, reaching up to 6 Mpa and to which CPB masses are subjected in deep mining operations. It serves to address a critical gap in experimental methodology, enabling the study of how CPB properties evolve under multiaxial high-stress compression within real mine field conditions. Figure 2 depicts the configuration of the apparatus that has been developed. This apparatus comprises two key components: i) the multiaxial compressive stress loading system, and ii) a customized sample cell that is equipped with a range of sensors and a drainage system.

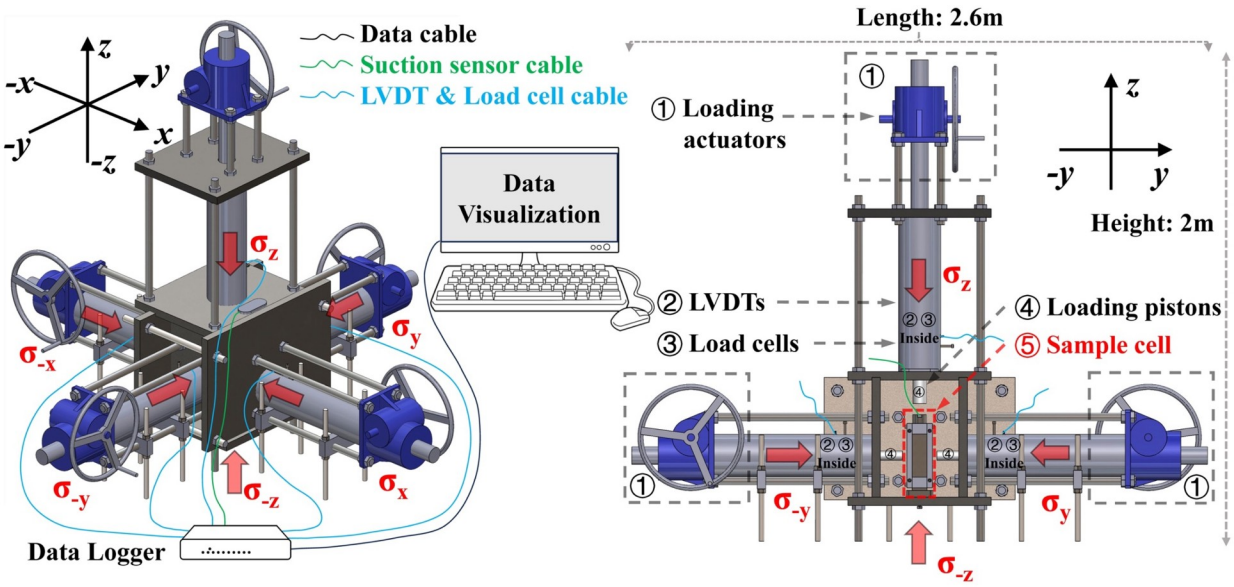


(a). Isometric view (b). Cutaway view

Figure 2. Schematic diagram of the multiaxial compressive stress curing and monitoring apparatus: a) isometric view, and b) cutaway view.

*MCS loading system*

The apparatus is comprised of five loading actuators (Figure 2a), each equipped with a loading cell and a Linear Variable Differential Transformer (LVDT) for precise stress measurement on the CPB sample and corresponding deformations. This setup applies MCS by incorporating two horizontal stresses that simulate horizontal compression from rockwall closure and vertical stress representing the combined impact of CPB self-weight and overburden pressure from rocks above. For clarity, we use notations (σ) to label stresses from different actuators and the rigid bottom plate, with each direction handling up to 6 MPa of loading. The actuators are manually operated to apply MCSs, and real-time stress and deformation data are efficiently captured by signal transducers. These data are seamlessly connected to a computer for comprehensive record-keeping and subsequent analysis. In Figure 2b, a customized sample cell is precisely centered within a sealed chamber designed to withstand the multiaxial loading from the five loading pistons.

*Customized sample cell equipped with sensors and a drainage system*

The custom-designed sample cell (Figure 3), comprises a detachable stainless-steel enclosure and a rubber membrane tailored to specific dimensions. The rubber membrane, with internal dimensions of 160 × 54 × 54 mm and a thickness of 1 mm, encapsulates the fresh CPB sample to prevent leaks. After undergoing curing under time-dependent MCS, the CPB sample is cut to the required 50 mm × 50 mm × 50 mm dimensions for UCS testing following ASTM C109 2020. A top opening in the rubber membrane is for

accommodating a sensor for monitoring temperature and matric suction within the CPB sample. This paper does not include or discuss data from the sensor.

The sample cell assembly includes a frame, bottom plate, four movable sidewalls, top plate, and loading connector. The frame, constructed with square bars and short plates, supports six loading plates aligned with six directions for load transfer. The beveled edges of these loading plates allow independent movement during compression, ensuring effective contact between the CPB and the loading plates. The stainless-steel construction prevents rust-induced issues and facilitates easy sampling and demolding. Figure 3c shows the bottom plate with a drainage control system comprising a seepage stone, drainage path, and drainage valve. In tests involving drainage, the CPB sample is enclosed with a rubber membrane featuring a circular opening on the bottom side, precisely aligned with the seepage stone. This design ensures a snug fit with the seepage stone. Subsequently, the drainage valve is opened, and a tube is connected to a collection bottle to gather the drainage water. Conversely, in undrained tests a sealed rubber membrane is employed to encase the CPB sample, and the drainage valve remains closed. This configuration ensures precise control over drainage conditions during the tests. In this paper, our experiments exclusively focus on tests that do not involve drainage.

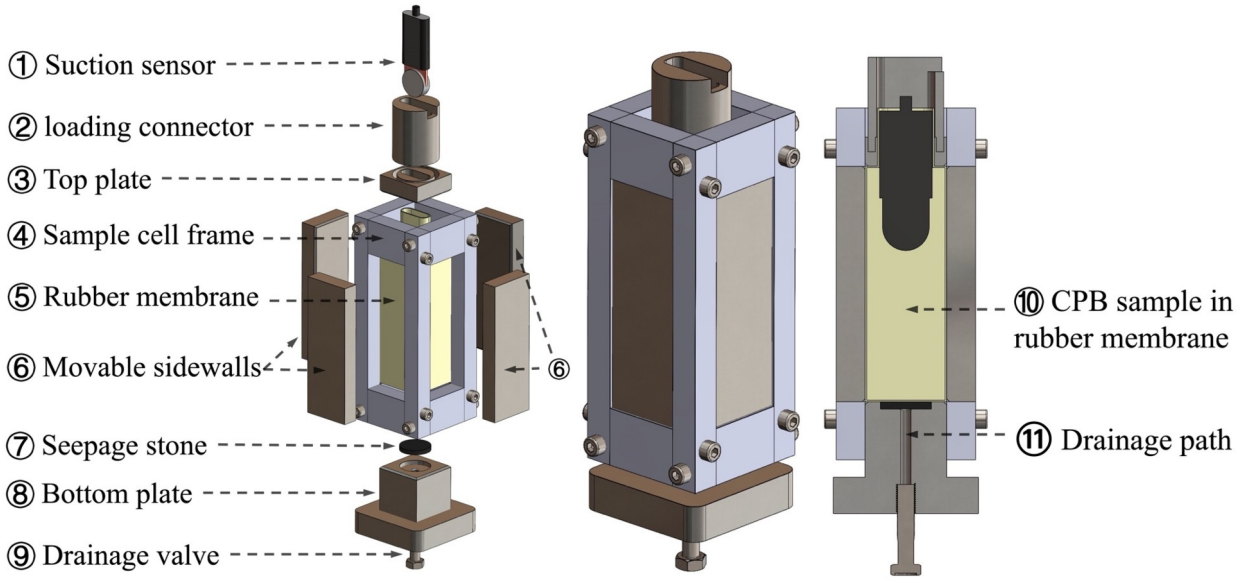


Figure 3. Schematic diagram of the customized sample cell: a) exploded view, b) collapsed view, and c) cutaway view.

**Experimental Program**

**Materials**

To address uncertainties related to the impact of chemical substances in natural tailings on CPB cement hydration, we utilized silica tailings (ST) in formulating the fresh CPB. These STs are derived from finely ground silica with a composition of 99.8% silicon dioxide ($SiO_2$). The physical characteristics of silica tailings are detailed in Table 1. In Figure 4, the particle size distribution (PSD) of ST is presented, showcasing a notable similarity to the PSD of natural tailings obtained from nine distinct mines in Canada. General Use Portland Cement (GU), the cement most commonly used in backfill operations in Canada, was used in this study. The characteristics of the GU used are listed in Table 2. Tap water was used to prepare the CPB.

Table 1. Physical properties of the silica tailings.

| Element | $G_s$ | $D_{10}$ (µm) | $D_{30}$ (µm) | $D_{50}$ (µm) | $D_{60}$ (µm) |
|---|---|---|---|---|---|
| Silica tailings | 2.7 | 1.9 | 9.0 | 22.5 | 31.5 |

Table 2. Characteristic of GU.

| Type of binder | MgO (%) | CaO (%) | $SiO_2$ (%) | $Al_2O_3$ (%) | $Fe_2O_3$ (%) | $SO_3$ (%) | Relative density, Gs | Specific surface ($m^2/g$) |
|---|---|---|---|---|---|---|---|---|
| GU | 2.65 | 62.82 | 18.03 | 4.53 | 2.70 | 3.82 | 3.10 | 1.30 |

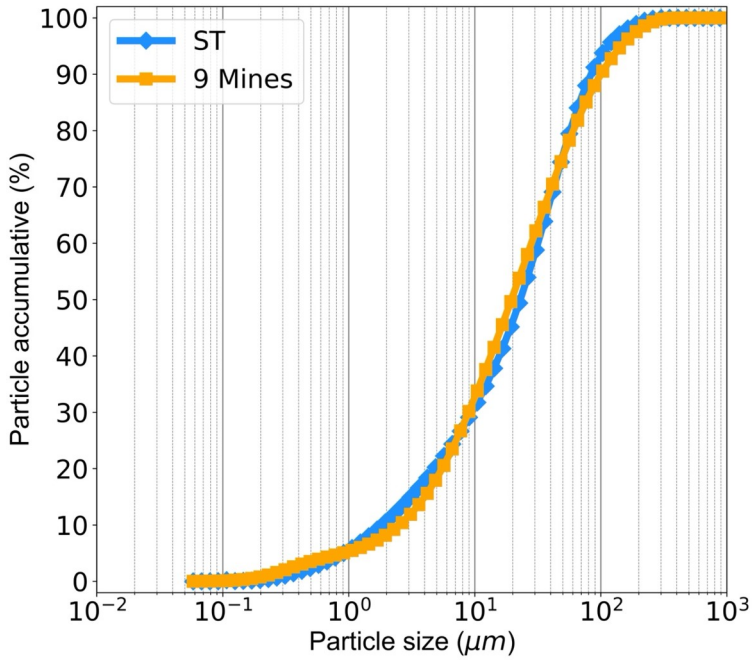


Figure 4. Particle size distribution of the silica tailings.

**Mix proportioning and sample preparation**

The CPB mixture used in this study consists of 7% GU relative to the total mass of fresh CPB. Additionally, the mixture has a concentration ratio defined as the solid mass (GU and ST) divided by the total mass, set at 74%. To achieve uniformity, GU, ST, and water were meticulously blended in a concrete mixer for 10 mins. Subsequently, the freshly prepared CPB mix was carefully poured into the customized sample cell and subjected to the prescribed curing conditions (as detailed in the next section) using the MCS curing and monitoring apparatus. Throughout the series of experimental tests, the component proportions were consistently maintained. The consistency of the CPB mixes, assessed by a slump test following ASTM C143 2010, yielded a slump value of 18 cm, a common measure in paste backfilling operations.

**Curing conditions**

The CPB samples were subjected to two different scenarios using undrained conditions (Figure 5):

1. **Control curing scenario** The samples were cured under no applied stress at a room temperature of 20℃. This represents the conventional and commonly used approach for CPB curing.
2. **MCS curing scenario** The samples were curied under MCS, which included vertical self-weight ($\sigma_v$) and rockwall closure-induced horizontal stresses ( $\sigma_{H1}$ and $\sigma_{H2}$), while maintaining a room temperature of 20℃

Figure 5 depicts the application scheme for both vertical and horizontal stresses, aiming to simulate the increased vertical stress from mine stope backfilling and the development of horizontal stress due to rockwall closure; dashed lines represent the equivalent *in situ* stresses targeted within the backfill mass, while solid lines illustrate how these stresses were applied to the CPB samples using our specially designed apparatus. To accurately replicate the simulation of an actual rockwall closure with equivalent horizontal closure rates, we meticulously controlled the two horizontal stresses ($\sigma_{-x}$, $\sigma_x$) at identical rates. The real-time dependent horizontal closure stress was obtained from *in situ* measurements conducted by Raffaldi et al. (2019) at the Lucky Friday mine. The vertical stress ($\sigma_z$) was simulated by maintaining a backfill filling rate of 0.31 m per hour, eventually reaching a backfill height of 29.76 m. This approach effectively replicates the self-weight effect of the CPB.

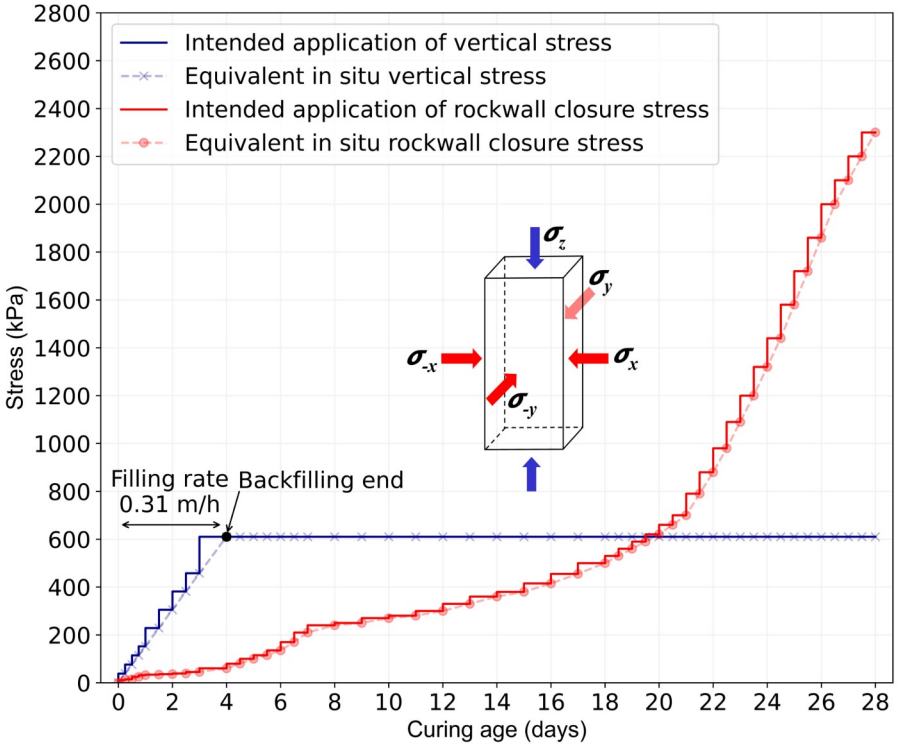


Figure 5. MCS curing conditions applied to the CPB samples during curing

**Testing and monitoring method**

*Compression tests*

After curing ages of 1, 3, 7, 14, and 28 days, the CPB samples were removed from the custom sample cell and cut to 50 × 50 ×50 mm cubes. The UCS of the cut CPB samples was determined in accordance with ASTM-C109 2020. The mechanical press has a normal load capacity of 50 kN. The loading rate was set at 1 mm/min. Each UCS strength test was conducted twice, and the average of the two measurements was considered as the unconfined compressive strength of the tested samples.

*Physical characterizations*

The physical characteristics of the samples mainly included parameters such as dry density ($\rho_d$), bulk density ($\rho_{bulk}$), void ratio (e), and porosity (n). After specific curing times, the samples were extracted, and their dimensions were recorded. After measurement, the samples were dried in a thermostatic oven maintained at a constant temperature of 45°C for a minimum of 4 days to eliminate free water. The mass of the dried samples was then determined, and considering initial volume and mass variations, gravimetric

water content (w), bulk density and dry density were calculated. Approximately 50 g of the dried sample was finely ground and used to determine specific gravity according to ASTM D854-14 2023. Void ratio and porosity can be determined on the basis of the specific gravity and initial volume of the CPB samples.

*Monitoring of multiaxial deformations*
The multiaxial deformations of the CPB under multiaxial compressive loading were measured by the LVDTs installed in the unit (Figure 2).

**Results and Discussion**
**Evolution of the multiaxial compressive curing stresses on CPB samples**
Multiaxial compressive curing stresses were applied per the stress program in Figure 5, with continuous monitoring using load cells. Figure 6 shows a close alignment between monitored MCS and scheduled curing stress curves, confirming apparatus accuracy. Interestingly, slight stress reduction occurred alongside CPB cured under multiaxial compressive stress condition (MCS-CPB) deformation after applying target stresses in each curing stage (Figure 11a). This precise stress control allows simulation of various multiaxial compression curing scenarios.

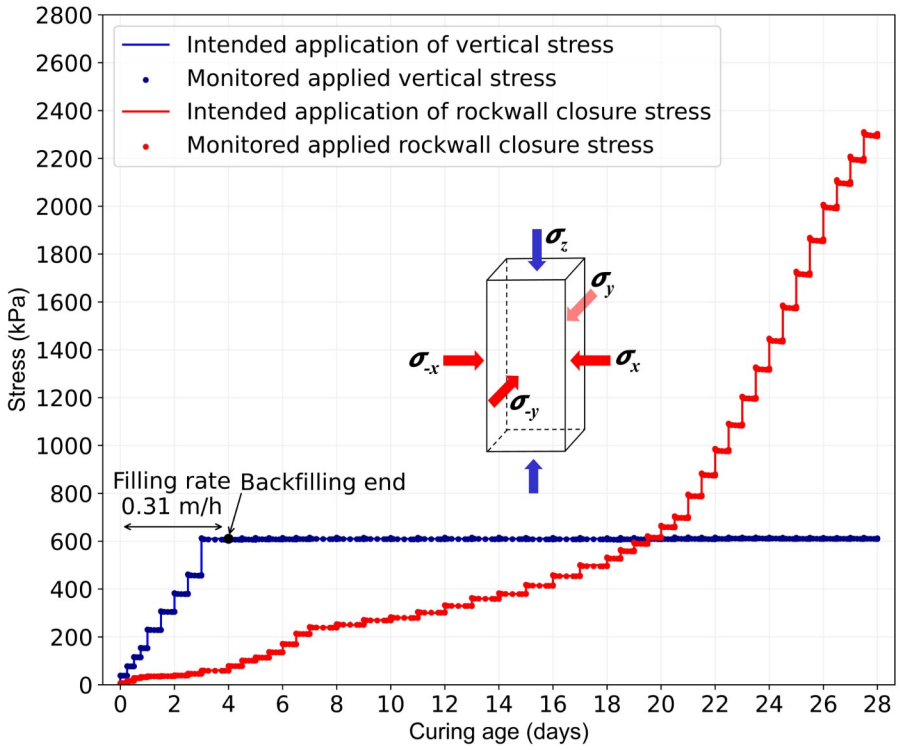


Figure 6. Applied and monitored MCS during curing process.

**Evolution of compressive strength and physical properties of CPB**
Figure 7 depicts the impact of multiaxial compressive stresses on the development of the unconfined compressive strength (UCS) of CPBs. As curing time progresses, the UCS of the Control-CPB shows a rapid increase during the early stage (0–7 days), followed by a slower rate of increase thereafter. In the early stages (0–7 days), cement hydration process occurred quickly and key hydration products, such as calcium silicate hydrate (C-S-H), calcium hydroxide (C-H), and ettringite were formed (Fall et al., 2010, Fall and Pokharel 2010). These hydration products help cement the tailings particles and refine the pore structure of CPB (Espinosa and Franke 2006, Ghirian and Fall 2015), resulting in the progressive

development of CPB strength over the curing period. This refinement was corroborated by the increase in dry density and decrease in porosity observed in the Control-CPB over the curing period, as shown in Figures 8a and 9a, respectively. Figure 8a shows that the dry density of the Control-CPB increased continuously from 1.430 g/cm³ at 1 day of curing age to 1.465 g/cm³ at 28 days of curing age. Simultaneously, the porosity of Control-CPB decreased from 0.468 to 0.439, as confirmed in Figure 9a. These concurrent increases in dry density and reductions in porosity provide strong evidence of a continuous process of pore refinement in CPB with curing age.

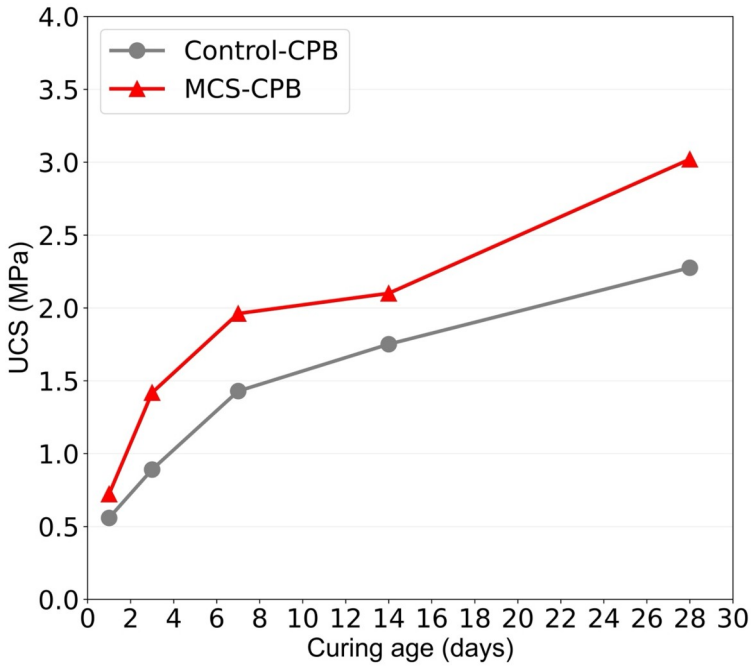


Figure 7. Variation in the UCS of Control-CPB and MCS-CPB as a function of curing age.

By contrast, the UCS of the MCS-CPB experienced a faster development during the first 7 days of curing, compared to the Control-CPB. At early curing age, the CPB was still in the process of hardening. The UCS of MCS-CPB exhibited considerable improvements, reaching 0.729, 1.412, and 1.954 MPa at 1, 3, and 7 days of curing age, respectively (Figure 7). These values represent enhancements of 30, 58, and 37% relative to the strengths of Control-CPB, which were 0.559, 0.891, and 1.429 MPa, respectively. The faster UCS development of MCS-CPB can be attributed to the effect of MCS. The rapid evolution of the vertical stress, corresponding to a filling rate of 0.31 m/hr, aids in particle setting, while the gradually increasing horizontal stresses from four distinct directions facilitate the densification of the MCS-CPB. These step-increasing stresses work in synergy to reduce the volume of void spaces, resulting in a volumetric strain of about 2.75% at the completion of backfilling (after 4 days of curing age), as depicted in Figure 11b. Furthermore, the porosity and void ratio results presented in Figure 9ab consistently indicate that the 'empty' space that exists within the MCS-CPB is less than that within the Control-CPB at all curing ages. In addition, the accelerated decrease in water content observed during the 0–7 days period (Figure 10) and the changes in bulk density (Figure 8b) of MCS-SCPB further corroborate the boosted cement hydration reaction at the early curing stage when compared to the Control-SCPB.

After the 7 days of curing age, the rate of UCS increase for MCS-CPB in 7–14 days period slows down much more than that for Control-CPB. Despite horizontal stresses increasing (from 210 kPa to 360 kPa) during this period, suggesting further refinement of MCS-CPB's pore structure, the 14 day UCS of MCS-CPB was only modestly improved by 7.8%, reaching 2.107 MPa. In contrast, the UCS of Control-CPB

maintains a substantial 22.5% improvement, increased from 1.429MPa at 7 days to 1.751MPa at 14 days. This implies that multiaxial compressive curing stresses accelerate early-phase (0–7 days) cement hydration, facilitating extensive hydration of cement particles and the accumulation of a large volume of hydration products. Consequently, this hinders subsequent hydration reactions during the later curing phase (7–14 days).

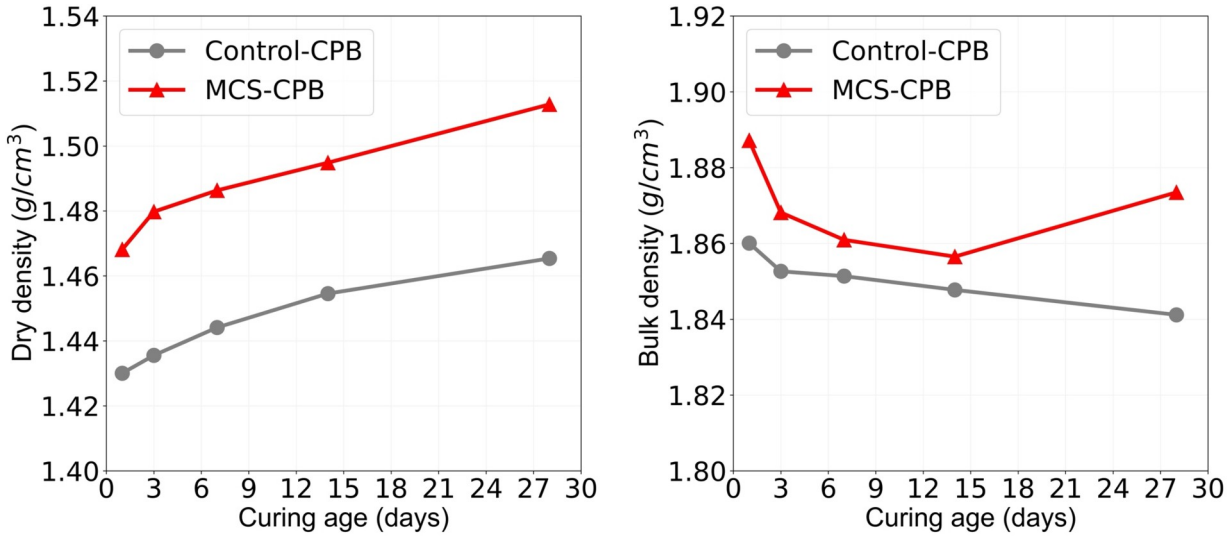


(a) Dry density (b) Bulk density

Figure 8. Evolution of density parameters over curing time for: a) Dry density, and b) bulk density.

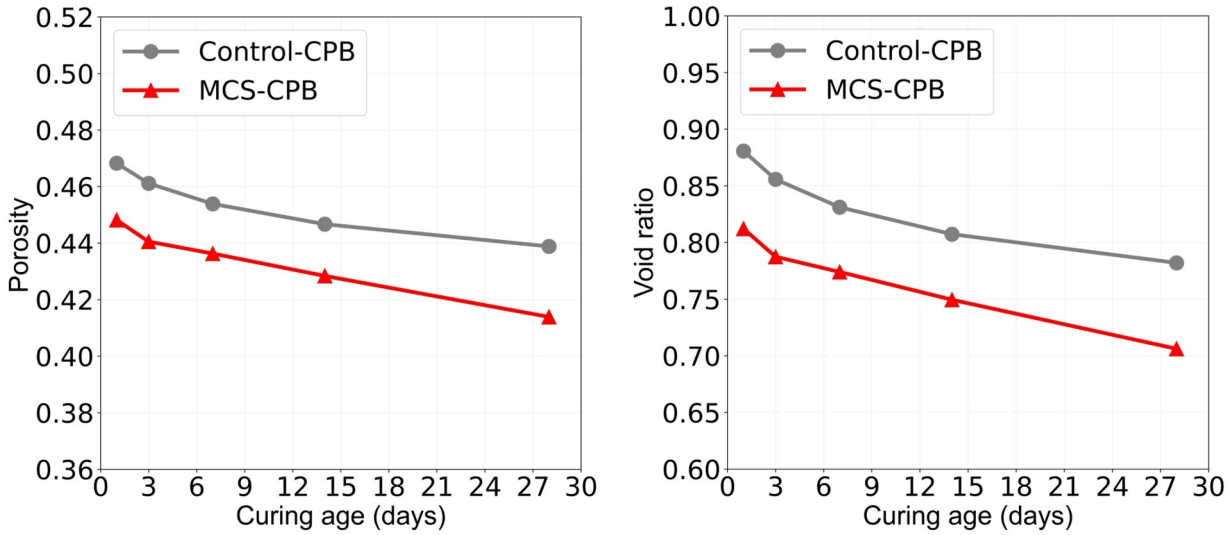


(a) Porosity (b) Void Ratio

Figure 9. Evolution of void characteristics over curing time for: a) porosity, b) void ratio.

Surprisingly, in the later phase (14–28 days), the rate of UCS increase for MCS-CPB improved even more than that of Control-CPB. By the 28th day of curing, the UCS of MCS-CPB reached 3.02 MPa, showing a 43% improvement, whereas the UCS of Control-CPB reached 2.276 MPa, indicating a 30% improvement compared to their respective 14 day UCS values. As discussed above, the compressive effect of the MCS already expedited early-phase (0–7 days) cement hydration, and a slowdown in cement hydration was

confirmed in the 7–14 days phase. The observed higher rate of UCS increase for MCS-CPB in the phase of 14–28 days was contributed by the much greater level of rockwall closure-induced horizontal stress. Figure 8b reveals that the bulk density of MCS-CPB reversed its decreasing trend (0–14 days) and reached 1.867 g/cm³ by the 28 days of curing age, up from 1.858 g/cm³ at 14 days. Additionally, the water content consumed in MCS-CPB from 14–28 days was less than that in Control-CPB (Figure 10). This suggests that while fewer cement hydration products may be produced inside MCS-CPB in the later phase (14–28 days), the MCS significantly densified the pore structure and improved particle interlock due to the higher time-dependent multiaxial stress. This densification is supported by the much lower porosity and void ratio of MCS-CPB at 28 days of curing (Figure 9ab).

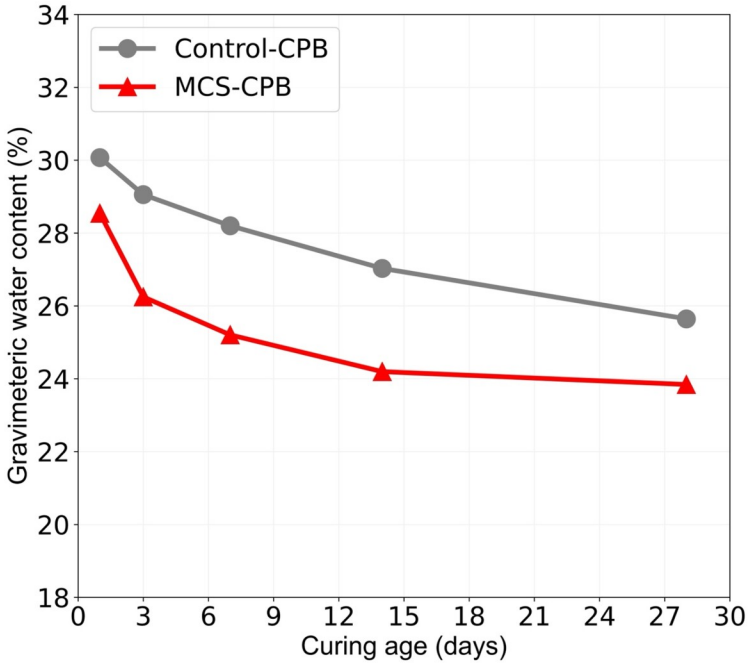


Figure 10. Evolution of gravimetric water content over curing time

**Evolution of the deformations and strains of the MCS-CPB**

As shown in Figure 11, the deformations and strains of MCS-CPB directly correlate with the applied stress in each axial direction. Notably, MCS-CPB exhibited rapid deformation upon each stress application, followed by a gradual and modest continuation until the application of next stress step. During the initial 7 day curing period, MCS-CPB demonstrated a dramatic increase in volumetric deformation, reaching 16.8 cm³ (equivalent to a volumetric strain of 3.62%). This deformation resulted from both the substantial increase in vertical stress in the 0–4 days phase and the discernible augmentation in horizontal stresses in the 4–7 days phase. Subsequently, spanning days 7–14, compressive volumetric deformation gradually increased to 18.8 cm³ (equivalent to a volumetric strain of 4.03%). This later compression phase was primarily driven by the amplification of horizontal stresses, rising from 210 kPa to 360 kPa during a period of 7–14 days. Despite the increasing magnitude of multiaxial stress, there was a progressive deceleration in the evolution of volumetric strain as the curing period advanced. This behaviour implies an increasing resistance of MCS-CPB to compression over time, indicative of improved hardness or stiffness. As shown in Figure 6, the applied horizontal stress exhibited a higher rate of increase after 14 days of curing, leading to the rapid development of horizontal deformations in MCS-CPB (Figure 11a). By the 28 days of curing age, the volumetric deformation of MCS-CPB reached 46.8 cm³ (equivalent to a volumetric strain of 10%). This substantial volumetric deformation further enhanced

the stiffness of MCS-CPB, contributing to an elevated UCS. This phenomenon also accounts for the increased rate of UCS during the later phase (14–28 days).

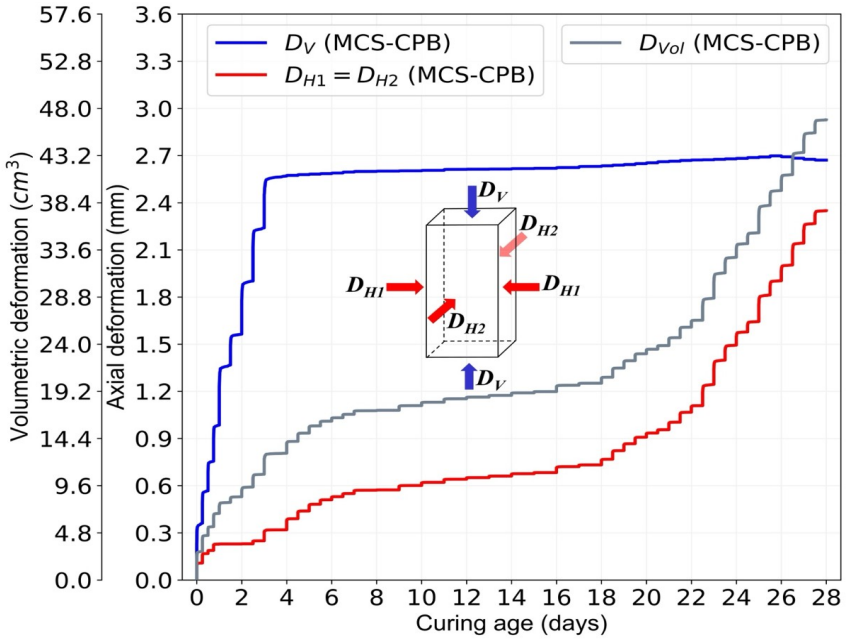


(a) Deformation

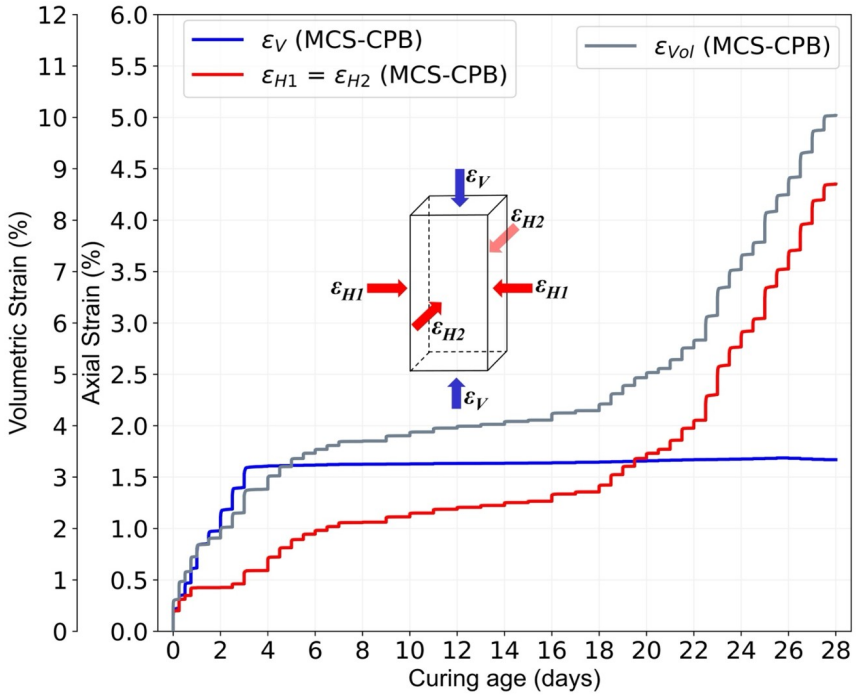


(b) Strain

Figure 11. Monitored deformations and calculated strains of the MCS-CPB during curing process during a) deformation ($D_V$: vertical deformation; $D_{H1}$, $D_{H2}$: horizontal deformation; $D_{vol}$: volumetric deformation), and (b) strain ($\varepsilon_V$: vertical strain; $\varepsilon_{H1}$, $\varepsilon_{H2}$: horizontal strain; $\varepsilon_{vol}$: volumetric strain).

## Summary and Conclusion

This study introduces a novel multiaxial compressive stress curing and monitoring apparatus designed for simulating paste backfilling in deep mining operations. The accuracy of this apparatus in simulating time-dependent MCS curing conditions has been validated. The MCS, including vertical stress from self-weight and rockwall closure-induced horizontal stresses, significantly impact the unconfined compressive strength and the physical properties of CPB. These stresses expedite initial cement hydration (0–7 days) and continually densify the pore structure of MCS-CPB, resulting in superior strength at all curing ages compared to stress-free CPB. Densification of MCS-CPB was confirmed by reduced void ratio and porosity, with notable contributions from rapidly increasing rockwall closure-induced horizontal stress during the later phase (14–28 days). Meticulous stress control enables the observation of compressive responses of MCS-CPB at each stress step throughout the curing process, providing insights into the evolution of deformation under time-dependent multiaxial stress conditions. MCS-CPB exhibited a progressive increase in volumetric deformation and strength over time, highlighting the positive impact of multiaxial stresses.

In summary, this new approach bridges the gap between laboratory experiments and *in situ* stopes in deep mine high stress environments, serving as a versatile tool for future research on the behaviour and performance of CPBs in multiaxial compressive stress conditions. For example, further studies examining the effect of different magnitudes and rate of stress increase induced by rock wall closure on CPB strength and mechanical damage are currently being carried out by the authors.

## Acknowledgements

The authors would like to thank the Natural Sciences and Research Council of Canada (NSERC), the University of Ottawa and the China Scholarship Council for their financial support.

### References

Arnold, D.A. 1993. An evaluation of cave mining in weak hanging wall conditions at hartebeestfontein gold mining company limited. University of the Witwatersrand.

Belem, T., Benzaazoua, M., Bussière, B., and Dagenais, A.M. 2002. Effects of settlement and drainage on strength development within mine paste backfill. *In* Proceedings of the Conference Tailings and Mine Waste'02. Fort Collins, Colorado, Balkema : Rotterdam. pp. 139–148.

Benzaazoua, M., Belem, T., and Yilmaz, E. 2006. Novel lab tool for paste backfill. Canadian Mining Journal, **127**(3): 31. Business Information Group, Don Mills.

Chen, S., Wu, A., Wang, Y., and Wang, W. 2021. Correlation of coupled effects of curing stress and curing temperature on the mechanical and physical properties of cemented paste backfill based on gray relational analysis. Arabian Journal of Geosciences, **14**(6): 479. doi:10.1007/s12517-021-06659-6.

Cui, L., and Fall, M. 2016. Mechanical and thermal properties of cemented tailings materials at early ages: Influence of initial temperature, curing stress and drainage conditions. Construction and Building Materials, **125**: 553–563. doi:10.1016/j.conbuildmat.2016.08.080.

Espinosa, R.M., and Franke, L. 2006. Influence of the age and drying process on pore structure and sorption isotherms of hardened cement paste. Cement and Concrete Research, **36**(10): 1969–1984. doi:10.1016/j.cemconres.2006.06.010.

Fall, M., Célestin, J.C., Pokharel, M., and Touré, M. 2010. A contribution to understanding the effects of curing temperature on the mechanical properties of mine cemented tailings backfill. Engineering Geology, **114**(3): 397–413. doi:10.1016/j.enggeo.2010.05.016.

Fall, M., and Ghirian, A. 2014. Coupled thermo-hydro-mechanical-chemical processes in cemented paste backfill and implications for backfill design – experimental results. *In* Proceedings of the Eleventh International Symposium on Mining with Backfill. Australian Centre for Geomechanics, Perth. pp. 183–196.

Fall, M., and Pokharel, M. 2010. Coupled effects of sulphate and temperature on the strength development of cemented tailings backfills: Portland cement-paste backfill. Cement and Concrete Composites, **32**(10): 819–828. doi:10.1016/j.cemconcomp.2010.08.002.

Ghirian, A., and Fall, M. 2015. Coupled behavior of cemented paste backfill at early ages. Geotechnical and Geological Engineering, **33**(5): 1141–1166. doi:10.1007/s10706-015-9892-6.

Ghirian, A., and Fall, M. 2016. Strength evolution and deformation behaviour of cemented paste backfill at early ages: Effect of curing stress, filling strategy and drainage. International Journal of Mining Science and Technology, **26**(5): 809–817. doi:10.1016/j.ijmst.2016.05.039.

Grabinsky, M., Jafari, M., and Pan, A. 2022. Cemented Paste Backfill (CPB) Material Properties for Undercut Analysis. Mining, **2**(1): 103–122. Multidisciplinary Digital Publishing Institute. doi:10.3390/mining2010007.

Malan, D.F., and Basson, F.R.P. 1998. Ultra-deep mining : The increased potential for squeezing conditions.

Masniyom, M. 2009. Systematic Selection and Application of Backfill in Underground Mines.

Raffaldi, M.J., Seymour, J.B., Richardson, J., Zahl, E., and Board, M. 2019. Cemented paste backfill geomechanics at a narrow-vein underhand cut-and-fill mine. Rock Mechanics and Rock Engineering, **52**(12): 4925–4940. doi:10.1007/s00603-019-01850-4.

Seymour, J., Benton, D.J., Raffaldi, M., Johnson, J., Martin, L., Boltz, S., and Richardson, J. 2016. Improving ground control safety in deep vein mines. *In* 3rd International Symposium on Mine Safety Science and Engineering. Montreal. pp. 71–77.

Seymour, J.B., Martin, L.A., Raffaldi, M.J., Warren, S.N., and Sandbak, L.A. 2019. Long-term stability of a 13.7 × 30.5-m (45 × 100-ft) undercut span beneath cemented rockfill at the Turquoise Ridge Mine, Nevada. Rock Mechanics and Rock Engineering, **52**(12): 4907–4923. doi:10.1007/s00603-019-01802-y.

Seymour, J.B., Raffaldi, M.J., and Abraham, H. 2017. Monitoring the In Situ Performance of Cemented Paste Backfill at the Lucky Friday Mine. *In* Minefill 2017: Proceedings of the 12th International Symposium on Mining with Backfill. p. 15.